AAAS
Ultrafast Science
Volume 2022, Article ID 9893418, 9 pages
https://doi.org/10.34133/2022/9893418

Ultrafast Science
A SCIENCE PARTNER JOURNAL

Research Article

High-Harmonic Generation and Correlated Electron Emission from Relativistic Plasma Mirrors at 1 kHz Repetition Rate

Stefan Haessler,[1] Marie Ouillé,[1,2] Jaismeen Kaur,[1] Maïmouna Bocoum,[1] Frederik Böhle,[1] Dan Levy,[3] Louis Daniault,[1] Aline Vernier,[1] Jérôme Faure,[1] and Rodrigo Lopez-Martens[1]

[1]*Laboratoire d'Optique Appliquée, ENSTA Paris, CNRS, Ecole Polytechnique, Institut Polytechnique de Paris, 181 Chemin de la Hunière et des Joncherettes, 91120 Palaiseau, France*
[2]*Ardop Engineering, Cité de la Photonique, 11 Avenue de la Canteranne, Bât. Pléione, 33600 Pessac, France*
[3]*Department of Physics of Complex Systems, Weizmann Institute of Science, Rehovot 7610001, Israel*

Correspondence should be addressed to Stefan Haessler; stefan.haessler@cnrs.fr

Received 14 December 2021; Accepted 1 June 2022; Published 28 June 2022

We report evidence for the first generation of XUV spectra from relativistic surface high-harmonic generation (SHHG) on plasma mirrors at a kilohertz repetition rate, emitted simultaneously with energetic electrons. SHHG spectra and electron angular distributions are measured as a function of the experimentally controlled plasma density gradient scale length L_g for three increasingly short and intense driving pulses: 24 fs and $a_0 = 1.1$, 8 fs and $a_0 = 1.6$, and finally 4 fs and $a_0 \approx 2.1$, where a_0 is the peak vector potential normalized by $m_e c/e$ with the elementary charge e, the electron rest mass m_e, and the vacuum light velocity c. For all driver pulses, we observe correlated relativistic SHHG and electron emission in the range $L_g \in [\lambda/20, \lambda/4]$, with an optimum gradient scale length of $L_g \approx \lambda/10$. This universal optimal L_g-range is rationalized by deriving a direct intensity-independent link between the scale length L_g and an effective similarity parameter for relativistic laser-plasma interactions.

1. Introduction

Surface high-harmonic generation (SHHG) from relativistic plasma mirrors [1–4] is a promising method for greatly enhancing the power of attosecond light pulses. This is motivated by key properties that differentiate it from the established method based on high-harmonic generation in gases [5]. Since the medium is already highly ionized, SHHG has no inherent limitation for the driving intensity such that a large fraction of the energy of an ultrahigh intensity driving laser can be compressed into an attosecond electromagnetic pulse. This is expected to occur with extremely high, percent-level conversion efficiencies [6–9] when driven under strongly relativistic conditions with a normalized vector potential $a_0 = eA_0/m_e c \gg 1$ (a practical formula is $a_0 = \sqrt{I[\mathrm{Wcm^{-2}}]\lambda^2[\mu\mathrm{m}^2]/1.37 \times 10^{18}}$), where e is the elementary charge, m_e the electron rest mass, c the vacuum light velocity, A_0 the laser's peak vector potential, I its peak intensity, and λ its central wavelength. Reported experimental laser-to-XUV conversion efficiencies for plasma mirrors with $a_0 \gtrsim 1$ are $\sim 10^{-4}$ [10–13] for photon energies >20 eV but are expected to increase with higher-intensity drivers. Finally, relativistic SHHG produces intrinsically Fourier-limited attosecond pulses, such that the complete spectral bandwidth, from the spectral cutoff in the XUV (or even hard X-rays [14]) all the way down to lowest harmonics and even the fundamental laser frequency, can contribute to the formation of attosecond pulses without costly spectral filtering and compression [15–17].

Reaching the relativistic SHHG regime with $a_0 > 1$ requires an on-target intensity of $\gtrsim 10^{18}\,\mathrm{W/cm^2}$ for an

800 nm laser while retaining a very steep surface plasma density profile

$$n(x) = n_c \exp\left[\frac{x}{L_g}\right], \quad (1)$$

with a scale length L_g of a small fraction of the driving laser wavelength λ. Here n_c is the nonrelativistic critical plasma density for the driving wavelength, and x is the coordinate in the target normal direction. Technically, this requires a highly focusable terawatt-class laser with a temporal contrast of $\gtrsim 10^{10}$. These conditions are typically met by Joule-class amplifier chains with dedicated contrast filters [18–21] and operating at $\lesssim$10 Hz repetition rate [8, 10–13, 20, 22].

Many applications as well as parametric studies of this regime would benefit from a higher repetition rate. At LOA, we have developed a unique laser chain with a power-scaled hollow-core-fiber postcompression system [23, 24] operating at 1 kHz repetition rate. Using this kHz laser, which achieves ultrahigh intensities with few-mJ pulse energy and few-cycle pulse duration, we have demonstrated laser-plasma interaction in the relativistic regime through laser-wakefield acceleration of electrons, both in underdense gas jets [25, 26] and in the underdense part of a smooth plasma density gradient on a plasma mirror [27]. Here, we report on the first experimental demonstration of relativistic SHHG at kHz repetition rate, the arguably most demanding application in terms of laser performance, as it depends critically on the spatiotemporal pulse quality and the temporal contrast.

1.1. High-Harmonic Generation on Plasma Mirrors. For relativistic driving intensities, $a_0 \gtrsim 1$, the SHHG emission mechanism is described by a push–pull process [28], also dubbed "relativistic electron spring" [29, 30], repeating once per driving laser period. The laser field first pushes electrons into the plasma, piling up a dense electron bunch and creating a restoring internal plasma field. As the laser field changes sign, the combined plasma and laser fields accelerate the electron bunch to a relativistic velocity towards the vacuum. SHHG emission then either results from a pure phase modulation of the incident laser field by the relativistically moving critical-density plasma surface ("relativistic oscillating mirror" (ROM)) [6, 15, 31] or as a coherent synchrotron emission (CSE) from the dense relativistic electron bunch as it gets accelerated orthogonally by the laser electric field [7, 9, 32].

For $a_0 \sim 1$, this relativistic SHHG emission needs to be discriminated from coherent wake emission (CWE) [4, 33], generated already at subrelativistic intensities, $a_0 < 1$. Once per laser field cycle, Brunel electrons [34] are accelerated out and back into the surface plasma, to form via collective trajectory crossings an electron density peak traversing the overdense part $(n(x) > n_c)$ of the plasma density gradient. In its wake, it excites plasma oscillations at the local plasma frequency which finally leads to the emission of one attosecond light pulse per laser cycle. Clear criteria are known for the discrimination of the two types of SHHG emission.

(i) Intensity dependence

The laser-to-SHHG conversion efficiency of CWE is constant over a large intensity range $>10^{15}$ W/cm^2 [4], whereas that of relativistic SHHG increases rapidly over a large a_0-range from $a_0 \sim 1$ until a saturation in the ultra-relativistic limit $a_0 \sim 100$ [4, 9]. Note however that in this experimentally still out-of-reach ultra-relativistic regime, the radiation reaction force may significantly modify SHHG [35].

(ii) Phase properties

The intensity dependence of the Brunel trajectories leads to increasing delays between successive attosecond pulses under the driving pulse envelope and thus to frequency-broadened negatively chirped individual CWE harmonics [33, 36]. A positively chirped driving pulse can partially compensate the effect and consequently lead to spectrally narrower CWE harmonics [33, 37, 38]. In contrast, for moderate $a_0 \sim 1$, the relativistic SHHG emission is Fourier-limited [4, 17] such that despite its much steeper intensity dependence and consequently shorter temporal envelope, its harmonic spectral width is narrower than that of CWE harmonics generated in the same conditions [4, 20, 39]. Only for higher $a_0 \gtrsim 10$, while the individual attosecond pulses remain Fourier-limited, plasma surface denting will again lead to a varying pulse-spacing and thus induce an intrinsic harmonic chirp, with the opposite sign compared to that of CWE [4, 40, 41].

(iii) Dependence on the plasma density gradient

The density gradient of the plasma-vacuum interface is a most crucial parameter [42], and its experimental control is a prerequisite for efficient SHHG [10, 22, 39]. In CWE, the electron density peak formation and conversion of plasma oscillations into XUV light are optimized for a very steep gradient with scale length $L_g \sim \lambda/100$. A growing L_g causes the CWE efficiency to drop rapidly [4] while the harmonic chirp and thus spectral width of the CWE-harmonic peaks increase [33, 37]. For the steep gradients optimizing CWE, relativistic SHHG is suppressed by the gyromagnetic effect [43] preventing electrons from escaping the plasma. Instead, relativistic SHHG has repeatedly been found in single-shot experiments to be optimized by smoother optimal density gradients [8, 10, 22, 39, 44], characterized by scale lengths $L_g \approx \lambda/10$. For further increased $L_g \gtrsim \lambda/4$, SHHG disappears due to the onset of chaotic electron dynamics [8, 22].

(iv) Simultaneous electron emission

Plasma mirrors also emit electron beams near the specular direction but slightly deviated toward the target normal [45, 46]. The same optimal $L_g \approx \lambda/10$ has been found to maximize the charge of relativistic electron bunches emitted from plasma mirrors [47], which is thus found to be correlated with relativistic SHHG [8, 28] and anticorrelated with CWE [48].

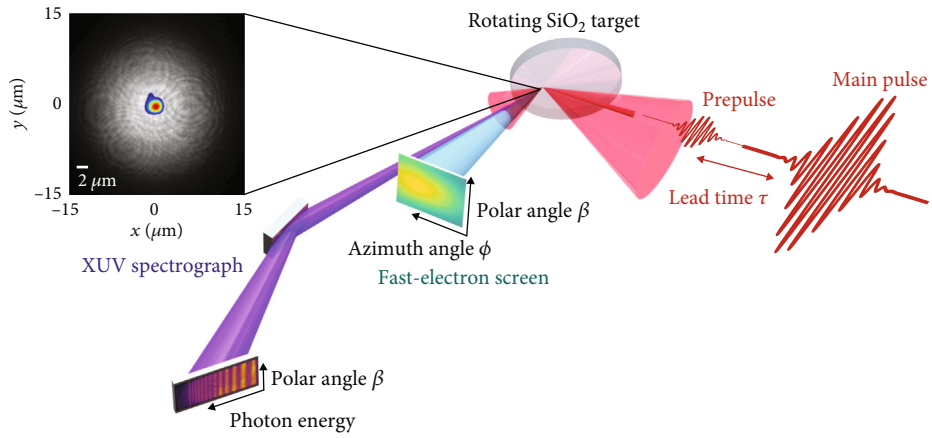

FIGURE 1: Schematics of the experimental setup for SHHG and electron acceleration on a kHz plasma mirror. The inset shows the on-target intensity profiles of the prepulse (in greyscale) and the main pulse (in colorscale).

2. Materials and Methods

The experiments were carried out using the 1 kHz "Salle Noire" laser system at LOA, delivering pulses with durations adjustable between 24 fs and <4 fs and a temporal contrast $>10^{10}$ at 10 ps [24]. As illustrated in Figure 1, the p-polarized pulses are focused down to a ≈1.8 μm FWHM spot by an f/1.3, 30° off-axis parabola onto a rotating optically flat fused-silica target at an incidence of $\theta = 55°$. With the pulse energy of 2.6 mJ on target, the measured spatial and temporal profiles yield, in the assumed absence of spatiotemporal couplings, peak intensities of 2.5×10^{18} W/cm^2 ($a_0 = 1.1$ for $\lambda = 800$ nm), 5.5×10^{18} W/cm^2 ($a_0 = 1.6$ for $\lambda = 800$ nm), and 1.0×10^{19} W/cm^2 ($a_0 = 2.1$ for $\lambda = 770$ nm) for 24 fs, 8 fs, and 4- fs pulses, respectively.

We thus operate in an intensity regime where both CWE and relativistic SHHG are expected to give significant contributions to the generated harmonic signal. Controlling the plasma density gradient scale length lets us modulate their weights [39]. To this end, a spatially superposed prepulse with lead time τ is focused to a 13 μm FWHM spot in order to prepare a plasma density gradient scale length $L_g = L_0 + c_s\tau$ [39, 49]. The expansion speed c_s is measured using spatial-domain interferometry (SDI) [49], and L_0 is the scale length increase owing to the finite temporal contrast of the main pulse. Our observation of CWE (see below) justifies the assumption that $L_0 \lesssim \lambda/50$ [4, 39].

The emitted SHHG radiation in the specular direction is recorded using an angle-resolving XUV spectrograph (cf. Figure 1), home-built with a gold-coated flat-field grating (600 lines/mm, 85.3° incidence) and a microchannel-plate (MCP) and phosphor screen detector. The MCP is time-gated for ≈250 ns synchronously with the laser pulses so as to suppress the detection of longer background plasma emission. The phosphor screen is finally imaged by a charged-coupled-device (CCD) camera to record angle-resolved ($\beta \in [-35, 35]$ mrad) SHHG spectra. This only detects the central part of the SHHG beam, which in our conditions has a FWHM divergence of ≈70 mrad, owing in particular to the small source spot. The SHHG spectra shown in the following are angle-integrated over the full detected range and represent the MCP signal without correction for the spectrometer's spectral response so as to enhance the visibility of the higher harmonic orders.

Simultaneously, we detect the angular emission profile of electrons with energies >150 keV with a lanex-screen [50] covered by a 15 μm aluminium foil, placed between the specular and the target-normal directions and imaged by a CCD camera (cf. Figure 1). The distributions along the azimuthal angle ϕ (in the incidence plane) shown in the following are integrated over the polar angle $\beta \in [-15°, 15°]$ (perpendicular to the incidence plane).

All shown data are acquired by integrating over 100 ms long bursts of pulses at 1 kHz repetition rate. The carrier-envelope phase (CEP) of the laser pulses has not been locked in this work. Its rapid random variation during these 100-shot acquisitions thus averages out CEP effects on the SHHG [13, 16, 51] and electron emission.

3. Results

Figure 2(a) shows results obtained with a near-Fourier-limited 24 fs driver pulse. The prepulse lead time is scanned on the ps-timescale, which translates via an SDI measurement to a change of plasma density gradient scale length from L_0 to $L_0 + \lambda/5$, where $\lambda = 800$ nm. Two L_g regimes are clearly distinguished. At the shortest gradients, $L_g - L_0 < \lambda/25$, the harmonic peaks are broad and their intensity quickly drops with increasing L_g, as expected for CWE emission. At higher L_g, the harmonic peaks are remarkably narrower and their intensity goes through an optimum located at $L_g - L_0 \approx \lambda/10$, consistent with the theoretical expectations for relativistic SHHG as well as with earlier experimental observations with similar multicycle driver pulses [8, 10, 39, 44]. No harmonics are visible beyond the CWE cutoff at 30 eV, which is not very surprising as the laser intensity is only just around the relativistic threshold, $a_0 = 1.1$. Finally, we find a stronger electron emission at softer gradients, correlated to the (presumed) relativistic SHHG emission.

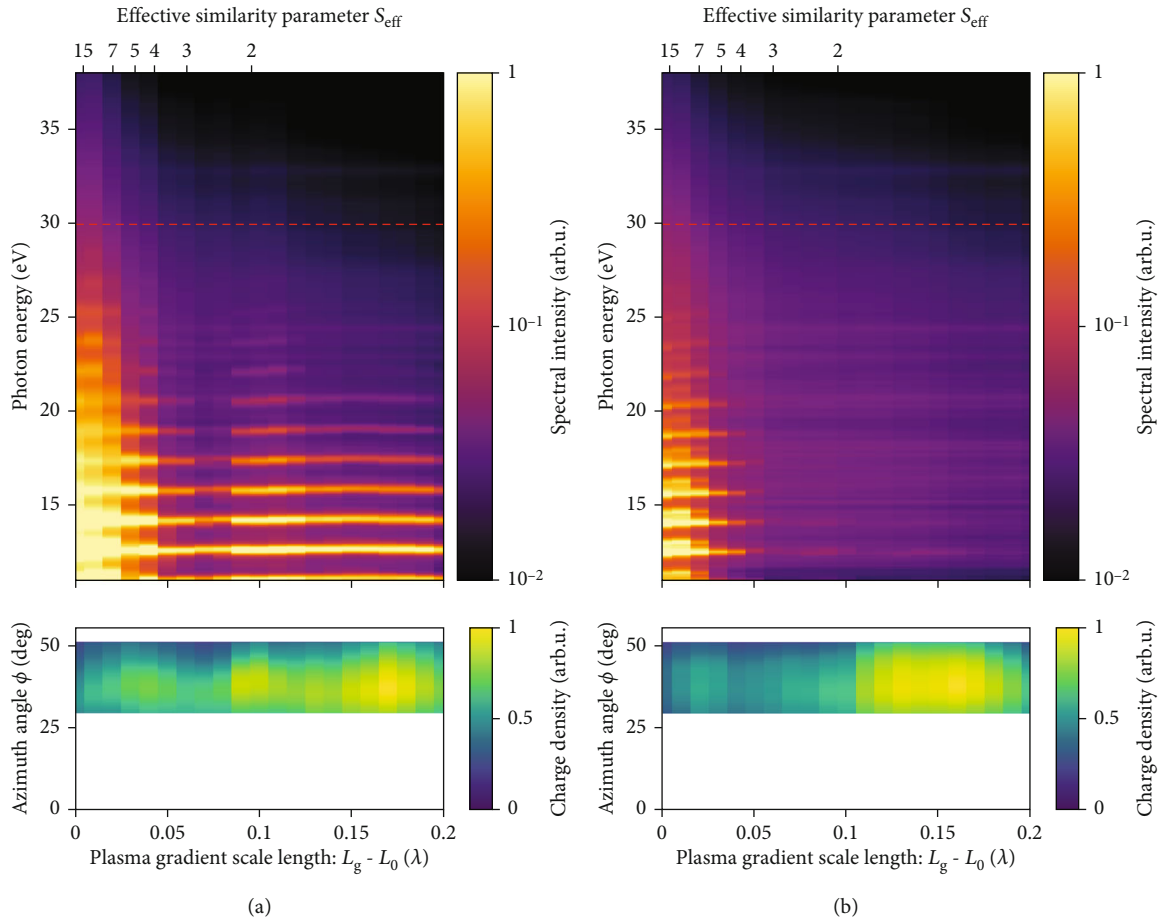

FIGURE 2: Synchronously measured SHHG (upper, log scale) and electron (lower) emission as a function of the plasma density gradient scale length. The dashed red line marks the CWE cutoff energy. The normal and specular directions correspond to $\phi = 0$ and $\phi = 55°$. (a) For a compressed, 24 fs, $a_0 = 1.1$ driver pulse, and (b) for the same pulse with added 500 fs^2 GDD, 85 fs duration, $a_0 = 0.6$. The upper horizontal axis gives S_{eff} corresponding to L_g as given by equation (3) and assuming $L_0 = \lambda/100$.

We can corroborate this interpretation by using a "Dazzler" acousto-optic programmable dispersive filter [52] in our amplifier chain to add 500 fs^2 GDD to the driving pulses, thus chirping them positively. This stretches them to 85 fs duration and consequently decreases the intensity to 0.7×10^{18} W/cm^2 ($a_0 = 0.6$ for $\lambda = 800$ nm). As shown in Figure 2(b), the harmonic spectral widths decrease significantly at the shortest L_g, but remain similar in intensity. This is consistent with the compensation of the aperiodicity of the CWE attosecond pulse train and the constant CWE conversion efficiency. The disappearance of the SHHG emission at softer gradients is consistent with the highly nonlinear intensity-dependence of relativistic SHHG. Electrons are still emitted preferentially for the softer gradients and the resulting anti-correlation of harmonics and electrons is reminiscent of our earlier sub-relativistic-intensity results [48].

Reducing the driving pulse duration to 8 fs at constant pulse energy increases the peak normalized vector potential to $a_0 = 1.5$ and leads to the results shown in Figure 3. As for the 24 fs driver, optimal relativistic SHHG is observed around $L_g - L_0 \approx \lambda/10$, with a clear correlation with electron emission for softer gradients. Additionally, we now observe the spectral extent of the SHHG signal to reach and possibly slightly surpass the CWE cutoff. For longer L_g, the relativistic SHHG signal persists until $L_g - L_0 \approx \lambda/4$ but its intensity and spectral extent gradually decrease.

An even shorter 4 fs driving pulse is expected to strongly boost the SHHG signal beyond the CWE cutoff. Self-steepening in the helium-filled hollow-core fiber used for postcompression however reduces the central wavelength to $\lambda \approx 770$ nm so that the peak normalized vector potential only increases to $a_0 = 2.1$ at constant pulse energy. Furthermore, such short pulses become extremely sensitive to spatiotemporal couplings which can drastically reduce the achievable peak intensity. On many days, we thus observe reduced spectral extent of the SHHG spectra generated with $\lesssim$4 fs pulses as compared to those obtained with 8 fs pulses shown in Figure 3, as was the case for the experiments reported in ref. [16].

We did nonetheless succeed in recording datasets like that shown in Figure 4 with a 4 fs driving pulse and shot-to-shot randomly varying CEP. Similarly to the above results, relativistic SHHG is observed for plasma density gradient scale lengths between $L_g - L_0 \approx \lambda/20$ and $\lambda/4$, where

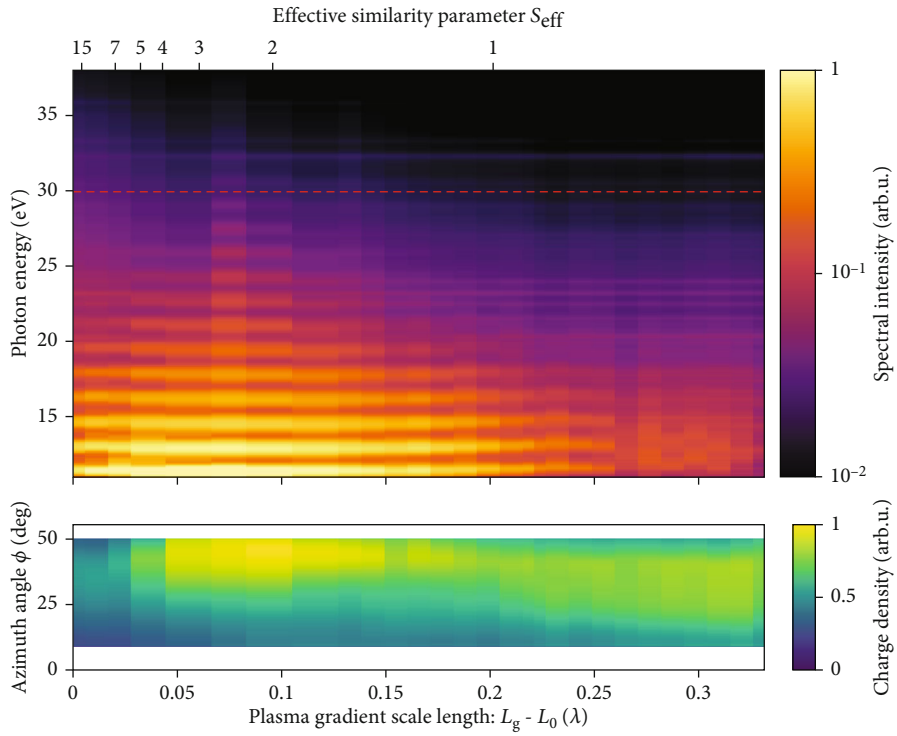

FIGURE 3: Synchronously measured SHHG (upper, log-scale) and electron (lower) emission as a function of the plasma density gradient scale length for an 8 fs, $a_0 = 1.6$ driver pulse. The dashed red line marks the CWE cutoff energy. The normal and specular directions correspond to $\phi = 0$ and $\phi = 55°$. The upper horizontal axis gives S_{eff} corresponding to L_g as given by equation (3) and assuming $L_0 = \lambda/100$.

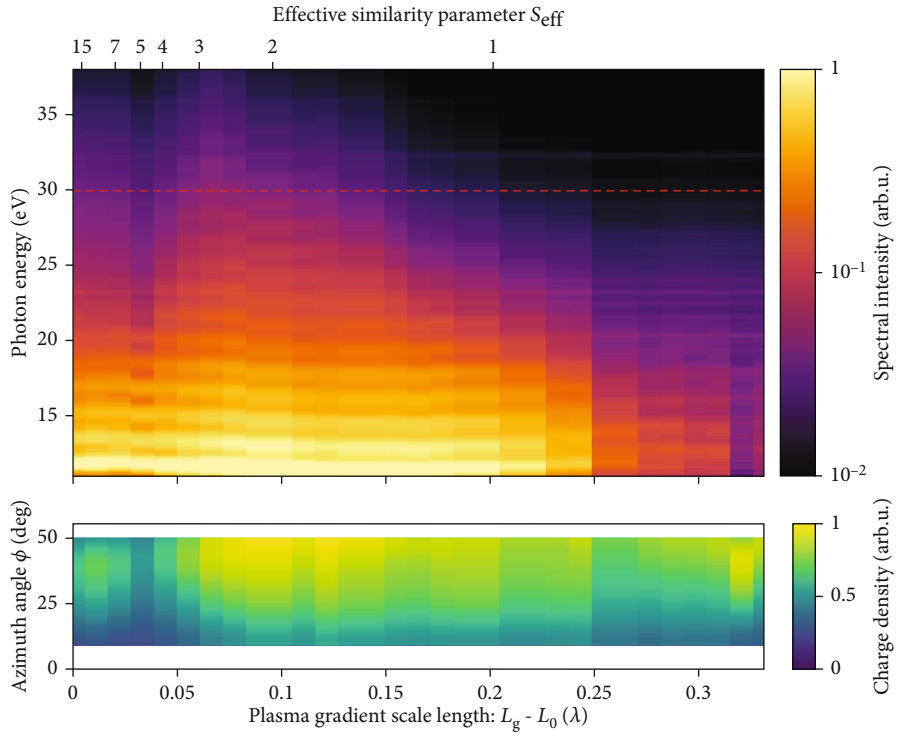

FIGURE 4: Synchronously measured SHHG (upper, log scale) and electron (lower) emission as a function of the plasma density gradient scale length for a 4 fs, $a_0 = 2.1$ driver pulse with $\lambda = 770$ nm central wavelength. The dashed red line marks the CWE cutoff energy. The normal and specular directions correspond to $\phi = 0$ and $\phi = 55°$. The upper horizontal axis gives S_{eff} corresponding to L_g as given by equation (3) and assuming $L_0 = \lambda/100$.

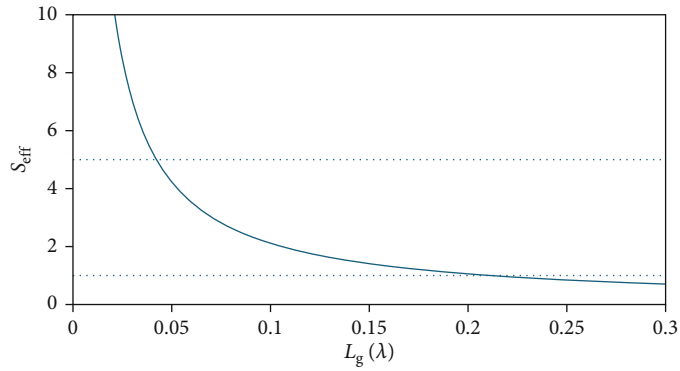

Figure 5: Theoretical intensity-independent effective similarity parameter S_{eff} (equation (3)) for $\theta = 55^\circ$ as a function of the scale length L_g of an exponential plasma density gradient (equation (1)). Dashed lines mark $S_{\text{eff}} = 1$ and $S_{\text{eff}} = 5$.

now $\lambda = 770$ nm. Around the optimal $L_g - L_0 \approx \lambda/10$, the spectra now extend well beyond the CWE cutoff, which is definite proof for relativistic SHHG, reported here for the first time with a 1 kHz repetition rate. The spectra still present a discernible harmonic modulation, in particular for the softer gradients, and one can make out small gradual L_g-dependent shifts of the harmonic peaks. These may result from a varying temporal structure of the generated very short (essentially 2-pulse [16]) attosecond-pulse-train. All recorded spectra are continuous, i.e., the harmonic peaks spectrally overlap, but their averaging over of random driver CEPs precludes us from inferring a temporal structure from spectral features [13, 16, 51].

The electron emission is again correlated with relativistic SHHG. Compared to Figures 2 and 3, we can make out that the electron beam is less clearly pushed away from the 55° specular direction, because of less efficient ponderomotive scattering of the electrons by the sub-2-cycle laser pulse as compared to the multicycle 8 fs and 24 fs pulses.

4. Discussion

We have found that relativistic SHHG occurs for plasma density gradient scale lengths $L_g \in [\lambda/20, \lambda/4]$, with an optimum at $L_g \approx \lambda/10$, with an assumed laser-contrast induced $L_0 \approx \lambda/100$. This optimum plasma gradient scale length is consistent with various earlier experiments with ≈30 fs laser drivers focused to higher $a_0 > 3$ [8, 10, 39, 44]. Here we find, for three different driving laser durations from 24 to 4 fs and lower peak intensities corresponding to $a_0 = 1.1$ to 2.1, the same optimal L_g-range. This apparent universality of the optimal plasma density gradient scale length is an intriguing observation.

In order to study density dependencies, particle-in-cell simulations often treat initially step-like plasma density profiles with variable peak density n. This adjusts the similarity parameter $S = n/(n_c a_0)$, which describes the relative strengths of the laser and induced internal plasma fields and scales laser-plasma interaction in the relativistic regime [53]. Optimal conditions for the relativistic push–pull process, relying on the formation and dynamics of a sharp electron density spike, are predicted for $S \in [1, 5]$ [9, 29, 30].

For currently explored experimental laser intensities, $a_0 \sim 1$, few-times overcritical plasma densities should thus be optimal. In solid-target experiments however, the plasma rather has $\sim 100 n_c$ bulk density, and the interaction rather occurs in the smooth density gradient at the surface. In the push-phase, the laser pulse sweeps electrons forward and penetrates this gradient up to a depth x_b, where the laser's Lorentz force and the electrostatic restoring force exerted by the plasma ion background are balanced [29, 30]. The plasma ion density at the depth x_b can then be taken to define an effective similarity parameter S_{eff}. This was demonstrated in ref. [54] with numerical simulations for a linear density ramp, with the core result that properties of SHHG obtained for a given S_{eff} match those obtained with a step-like plasma profile whose density satisfies $S = S_{\text{eff}}$.

Here, we take the same approach but consider instead the experimentally relevant exponential density profile of equation (1). In this plasma, the laser-plasma force balance yields an instantaneous penetration depth [28, 41] $x_b = L \ln[a(1 + \sin\theta)\cos\theta/\pi L/\lambda]$, where θ is the laser incidence angle on the plasma surface and $a = a_0 \cos(\varphi)$ is the instantaneous value of the normalized vector potential during the pushing half-cycle, i.e., $\varphi \in [-\pi/2, \pi/2]$. With the half-cycle averaged vector potential $(2/\pi)a_0$, we can define an effective penetration depth of

$$\bar{x_b} = L_g \ln\left[\frac{2a_0(1 + \sin\theta)\cos\theta}{\pi^2(L_g/\lambda)}\right]. \tag{2}$$

Experimentally varying the scale length L_g thus corresponds to adjusting the effective plasma (ion) density $n[\bar{x_b}(L_g)]$, where a larger L_g corresponds to a lower density. With this density, we find an effective similarity parameter

$$S_{\text{eff}} = \frac{n(\bar{x_b})}{n_c a_0} = \frac{2(1 + \sin\theta)\cos\theta}{\pi^2(L_g/\lambda)}. \tag{3}$$

It is remarkable that this is independent of the laser intensity and, for a given incidence angle, only depends on the gradient scale length. For a given exponential density profile and for any intensity that is sufficiently high to be

considered relativistic, the laser thus piles up the electrons at the depth where the ion density corresponds to the *same* similarity parameter. This direct correspondence of L_g and S_{eff} is the reason for the intensity-independent optimal L_g-range that we find in our experiments.

We plot S_{eff} from equation (3) for our experimental incidence angle $\theta = 55°$ in Figure 5. The theoretically predicted optimal range $S \in [1, 5]$ for relativistic SHHG [9, 29, 30] is thus achieved for $L_g \in [\lambda/25, \lambda/5]$. This is in excellent agreement with our experimentally observed intensity-*in*dependent L_g-range. Assuming $L_0 = \lambda/100$, equation (3) yields the S_{eff} axes in Figures 2–4.

5. Conclusion

We have reported clear evidence for the first observation of relativistic SHHG from plasma mirrors driven at kilohertz repetition rate. These are correlated to the emission of energetic electrons through the variation of the surface plasma density gradient scale length L_g. For three increasingly short and intense driving pulses (from 24 fs (9 optical cycles) and $a_0 = 1.1$ to 4 fs (1.7 optical cycles) and $a_0 \approx 2.1$), relativistic SHHG has been observed for the same L_g-range, $L_g \in [\lambda/20, \lambda/4]$, with an optimum gradient scale length of $L_g \approx \lambda/10$. The universality of the optimal L_g-range has been rationalized by deriving a direct intensity-independent link between the scale length L_g of an exponential plasma density profile and an effective similarity parameter for relativistic laser-plasma interactions. The observed optimal L_g-range corresponds very well to theoretically expected optimal similarity parameters.

These results open the route to a detailed examination and optimization of relativistic SHHG, exploiting the high kHz repetition rate and exceptional stability of our laser system [24] and next-generation systems in development [55]. In particular for the shortest pulse durations and with added CEP-locking, we should become able to harness the favorable phase properties of relativistic SHHG for the generation of powerful isolated attosecond pulses from ultraintense laser-driven plasma mirrors [13, 16, 51].

Data Availability

The data that support the findings of this study are available from the corresponding author, S.H., upon reasonable request.

Conflicts of Interest

The authors declare that there is no conflict of interest regarding the publication of this article.

Authors' Contributions

R.L.-M., J.F., and S.H. designed the research project. M.B., F.B., and S.H. built the SHHG setup, made preliminary experiments, and developed the data analysis routines. M.O., J.K. and A.V. operated the laser chain. M.O., J.K., L.D., D.L., and S.H. performed the experiments. S.H., M.O., and J.K. analyzed the data. S.H. wrote the paper, with support through comments from all authors.

Acknowledgments

This work was supported by the Agence Nationale pour la Recherche (ANR-11-EQPX-005-ATTOLAB and ANR-14-CE32-0011-03 APERO), Investissements d'Avenir Program LabEx PALM (ANR-10-LABX-0039-PALM), European Research Council (ERC FEMTOELEC 306708 and ERC ExCoMet 694596), Laserlab-Europe (H2020-EU.1.4.1.2. grant agreement ID 654148), and Région Ile-de-France (SESAME 2012-ATTOLITE).

References

[1] B. Dromey, M. Zepf, A. Gopal et al., "High harmonic generation in the relativistic limit," *Nature Physics*, vol. 2, no. 7, pp. 456–459, 2006.

[2] A. Tarasevitch, K. Lobov, C. Wünsche, and D. von der Linde, "Transition to the relativistic regime in high order harmonic generation," *Physical Review Letters*, vol. 98, no. 10, p. 103902, 2007.

[3] U. Teubner and P. Gibbon, "High-order harmonics from laser-irradiated plasma surfaces," *Reviews of Modern Physics*, vol. 81, no. 2, pp. 445–479, 2009.

[4] C. Thaury and F. Quéré, "High-order harmonic and attosecond pulse generation on plasma mirrors: basic mechanisms," *Journal of Physics B: Atomic, Molecular and Optical Physics*, vol. 43, p. 213001, 2010.

[5] F. Calegari, G. Sansone, S. Stagira, C. Vozzi, and M. Nisoli, "Advances in attosecond science," *Journal of Physics B: Atomic, Molecular and Optical Physics*, vol. 49, no. 6, p. 062001, 2016.

[6] G. D. Tsakiris, K. Eidmann, J. Meyer-ter-Vehn, and F. Krausz, "Route to intense single attosecond pulses," *New Journal of Physics*, vol. 8, p. 19, 2006.

[7] D. An der Brügge and A. Pukhov, "Enhanced relativistic harmonics by electron nanobunching," *Physics of Plasmas*, vol. 17, no. 3, p. 033110, 2010.

[8] L. Chopineau, A. Leblanc, G. Blaclard et al., "Identification of coupling mechanisms between ultraintense laser light and dense plasmas," *Physical Review X*, vol. 9, no. 1, p. 011050, 2019.

[9] M. R. Edwards and J. M. Mikhailova, "The X-ray emission effectiveness of plasma mirrors: reexamining power-law scaling for relativistic high-order harmonic generation," *Scientific Reports*, vol. 10, no. 1, pp. 1–20, 2020.

[10] C. Rödel, D. an der Brügge, J. Bierbach et al., "Harmonic generation from relativistic plasma surfaces in ultrasteep plasma density gradients," *Physical Review Letters*, vol. 109, no. 12, p. 125002, 2012.

[11] P. Heissler, A. Barna, J. M. Mikhailova et al., "Multi-μJ harmonic emission energy from laser-driven plasma," *Applied Physics B*, vol. 118, no. 2, pp. 195–201, 2015.

[12] M. Yeung, S. Rykovanov, J. Bierbach et al., "Experimental observation of attosecond control over relativistic electron bunches with two-colour fields," *Nature Photonics*, vol. 11, no. 1, pp. 32–35, 2017.

[13] O. Jahn, V. E. Leshchenko, P. Tzallas et al., "Towards intense isolated attosecond pulses from relativistic surface high harmonics," *Optica*, vol. 6, no. 3, pp. 280–287, 2019.

[14] B. Dromey, S. Kar, C. Bellei et al., "Bright multi-keV harmonic generation from relativistically oscillating plasma surfaces," *Physical Review Letters*, vol. 99, no. 8, p. 085001, 2007.

[15] S. Gordienko, A. Pukhov, O. Shorokhov, and T. Baeva, "Relativistic Doppler effect: universal spectra and zeptosecond pulses," *Physical Review Letters*, vol. 93, article 115002, 2004.

[16] F. Böhle, M. Thévenet, M. Bocoum, A. Vernier, S. Haessler, and R. Lopez-Martens, "Generation of XUV spectral continua from relativistic plasma mirrors driven in the near-single-cycle limit," *Journal of Physics: Photonics*, vol. 2, no. 3, p. 034010, 2020.

[17] L. Chopineau, A. Denoeud, A. Leblanc et al., "Spatio-temporal characterization of attosecond pulses from plasma mirrors," *Nature Physics*, vol. 17, no. 8, pp. 968–973, 2021.

[18] H. C. Kapteyn, M. M. Murnane, A. Szoke, and R. W. Falcone, "Prepulse energy suppression for high-energy ultrashort pulses using self-induced plasma shuttering," *Optics Letters*, vol. 16, no. 7, pp. 490–492, 1991.

[19] B. Dromey, S. Kar, M. Zepf, and P. Foster, "The plasma mirror—a subpicosecond optical switch for ultrahigh power lasers," *Review of Scientific Instruments*, vol. 75, no. 3, pp. 645–649, 2004.

[20] C. Thaury, F. Quéré, J. P. Geindre et al., "Plasma mirrors for ultrahigh-intensity optics," *Nature Physics*, vol. 3, no. 6, pp. 424–429, 2007.

[21] A. Jullien, O. Albert, F. Burgy et al., "10−10 temporal contrast for femtosecond ultraintense lasers by cross-polarized wave generation," *Optics Letters*, vol. 30, no. 8, pp. 920–922, 2005.

[22] F. Dollar, P. Cummings, V. Chvykov et al., "Scaling high-order harmonic generation from laser-solid interactions to ultrahigh intensity," *Physical Review Letters*, vol. 110, no. 17, p. 175002, 2013.

[23] F. Böhle, M. Kretschmar, A. Jullien et al., "Compression of CEP-stable multi-mJ laser pulses down to 4 fs in long hollow fibers," *Laser Physics Letters*, vol. 11, no. 9, p. 095401, 2014.

[24] M. Ouillé, A. Vernier, F. Böhle et al., "Relativistic-intensity near-single-cycle light waveforms at khz repetition rate," *Light: Science & Applications*, vol. 9, pp. 47–49, 2020.

[25] D. Guénot, D. Gustas, A. Vernier et al., "Relativistic electron beams driven by kHz single-cycle light pulses," *Nature Photonics*, vol. 11, pp. 293–296, 2017.

[26] D. Gustas, D. Guénot, A. Vernier et al., "High-charge relativistic electron bunches from a kHz laser-plasma accelerator," *Physical Review Accelerators and Beams*, vol. 21, no. 1, p. 013401, 2018.

[27] N. Zaïm, F. Böhle, M. Bocoum et al., "Few-cycle laser wakefield acceleration on solid targets with controlled plasma scale length," *Physics of Plasmas*, vol. 26, no. 3, p. 033112, 2019.

[28] M. Thévenet, H. Vincenti, and J. Faure, "On the physics of electron ejection from laser-irradiated overdense plasmas," *Physics of Plasmas*, vol. 23, no. 6, p. 063119, 2016.

[29] A. A. Gonoskov, A. V. Korzhimanov, A. V. Kim, M. Marklund, and A. M. Sergeev, "Ultrarelativistic nanoplasmonics as a route towards extreme-intensity attosecond pulses," *Physical Review E*, vol. 84, no. 4, p. 046403, 2011.

[30] A. Gonoskov, "Theory of relativistic radiation reflection from plasmas," *Physics of Plasmas*, vol. 25, no. 1, p. 013108, 2018, (visited on 02/06/2018).

[31] R. Lichters, J. Meyer-ter-Vehn, and A. Pukhov, "Short-pulse laser harmonics from oscillating plasma surfaces driven at relativistic intensity," *Physics of Plasmas*, vol. 3, no. 9, pp. 3425–3437, 1996.

[32] J. M. Mikhailova, M. V. Fedorov, N. Karpowicz et al., "Isolated attosecond pulses from laser-driven synchrotron radiation," *Physical Review Letters*, vol. 109, no. 24, p. 245005, 2012.

[33] F. Quéré, C. Thaury, P. Monot et al., "Coherent wake emission of high-order harmonics from overdense plasmas," *Physical Review Letters*, vol. 96, no. 12, p. 125004, 2006.

[34] F. Brunel, "Not-so-resonant, resonant absorption," *Physical Review Letters*, vol. 59, no. 1, pp. 52–55, 1987.

[35] S. Tang, N. Kumar, and C. H. Keitel, "Plasma high-order-harmonic generation from ultraintense laser pulses," *Physical Review E*, vol. 95, no. 5, p. 051201, 2017.

[36] K. Varjú, Y. Mairesse, B. Carré et al., "Frequency chirp of harmonic and attosecond pulses," *Journal of Modern Optics*, vol. 52, no. 2-3, pp. 379–394, 2005.

[37] A. Malvache, A. Borot, F. Quéré, and R. Lopez-Martens, "Coherent wake emission spectroscopy as a probe of steep plasma density profiles," *Physical Review E*, vol. 87, no. 3, p. 035101, 2013.

[38] A. V. Mitrofanov, D. A. Sidorov-Biryukov, P. B. Glek et al., "Chirp-controlled high-harmonic and attosecond-pulse generation via coherent-wake plasma emission driven by mid-infrared laser pulses," *Optics Letters*, vol. 45, no. 3, pp. 750–753, 2020.

[39] S. Kahaly, S. Monchocé, H. Vincenti et al., "Direct observation of density-gradient effects in harmonic generation from plasma mirrors," *Physical Review Letters*, vol. 110, no. 17, p. 175001, 2013.

[40] M. Behmke, D. an der Brügge, C. Rödel et al., "Controlling the spacing of attosecond pulse trains from relativistic surface plasmas," *Physical Review Letters*, vol. 106, no. 18, p. 185002, 2011.

[41] H. Vincenti, S. Monchocé, S. Kahaly, G. Bonnaud, P. Martin, and F. Quéré, "Optical properties of relativistic plasma mirrors," *Nature Communications*, vol. 5, p. 3403, 2014.

[42] M. Zepf, G. D. Tsakiris, G. Pretzler et al., "Role of the plasma scale length in the harmonic generation from solid targets," *Physical Review E*, vol. 58, p. R5253, 1998.

[43] J. P. Geindre, P. Audebert, and R. S. Marjoribanks, "Relativistic *AC* gyromagnetic effects in ultraintense laser-matter interaction," *Physical Review Letters*, vol. 97, no. 8, p. 085001, 2006.

[44] J. Gao, B. Li, F. Liu et al., "Double optimal density gradients for harmonic generation from relativistically oscillating plasma surfaces," *Physics of Plasmas*, vol. 26, no. 10, p. 103102, 2019.

[45] Y. Tian, J. Liu, W. Wang et al., "Electron emission at locked phases from the laser-driven surface plasma wave," *Physical Review Letters*, vol. 109, p. 115002, 2012.

[46] C. Zhou, Y. Bai, L. Song et al., "Direct mapping of attosecond electron dynamics," *Nature Photonics*, vol. 15, no. 3, pp. 216–221, 2021.

[47] M. Thévenet, A. Leblanc, S. Kahaly et al., "Vacuum laser acceleration of relativistic electrons using plasma mirror injectors," *Nature Physics*, vol. 12, no. 4, pp. 355–360, 2016.

[48] M. Bocoum, M. Thévenet, F. Böhle et al., "Anticorrelated emission of high harmonics and fast electron beams from plasma mirrors," *Physical Review Letters*, vol. 116, no. 18, p. 185001, 2016.

[49] M. Bocoum, F. Böhle, A. Vernier, A. Jullien, J. Faure, and R. Lopez-Martens, "Spatial-domain interferometer for measuring plasma mirror expansion," *Optics Letters*, vol. 40, p. 3009, 2015.

[50] Y. Glinec, J. Faure, A. Guemnie-Tafo et al., "Absolute calibration for a broad range single shot electron spectrometer," *Review of Scientific Instruments*, vol. 77, no. 10, p. 103301, 2006.

[51] D. Kormin, A. Borot, G. Ma et al., "Spectral interferometry with waveform-dependent relativistic high-order harmonics from plasma surfaces," *Nature Communications*, vol. 9, no. 1, p. 4992, 2018.

[52] F. Verluise, V. Laude, Z. Cheng, C. Spielmann, and P. Tournois, "Amplitude and phase control of ultrashort pulses by use of an acousto-optic programmable dispersive filter: pulse compression and shaping," *Optics Letters*, vol. 25, no. 8, pp. 575–577, 2000.

[53] S. Gordienko and A. Pukhov, "Scalings for ultrarelativistic laser plasmas and quasimonoenergetic electrons," *Physics of Plasmas*, vol. 12, p. 043109, 2005.

[54] T. G. Blackburn, A. A. Gonoskov, and M. Marklund, "Relativistically intense XUV radiation from laser-illuminated near-critical plasmas," *Physical Review A*, vol. 98, no. 2, p. 023421, 2018.

[55] S. Toth, T. Stanislauskas, I. Balciunas et al., "SYLOS lasers–the frontier of few-cycle, multi-TW, kHz lasers for ultrafast applications at extreme light infrastructure attosecond light pulse source," *Journal of Physics: Photonics*, vol. 2, p. 045003, 2020.